

## Probing the Debye Layer: Capacitance and Potential of Zero Charge Measured Using a Debye-Layer Transistor

J.-L. Fraikin, M. V. Requa, and A. N. Cleland

*Department of Physics, University of California, Santa Barbara, California, USA*

(Received 9 February 2009; published 16 April 2009)

We present a unique method for probing the properties of the electrolytic Debye layer, incorporating it as the active element in a novel radio frequency (rf) field-effect transistor. The capacitance of the Debye layer depends nonlinearly on the voltage applied across it, and we exploit this dependence to directly modulate the rf conductance between two nanofabricated interdigitated electrodes. We make quantitative measurements of the Debye-layer capacitance, allowing us to determine the potential of zero charge, a quantity of importance for electrochemistry and impedance-based biosensing.

DOI: 10.1103/PhysRevLett.102.156601

PACS numbers: 85.30.Tv, 73.30.+y, 82.45.Yz

The Debye layer is an accumulation of ions which forms on any charged surface immersed in an aqueous electrolyte [1] and has a thickness of the order 1–10 nm. Devices have been developed that employ the Debye layer as an active element [2], including nanofluidic diodes and bipolar junctions made using nanopores and nanochannels [3–5]. In these devices, chemical or electrical gating controls the charge carrier density within the Debye layer and so the channel conductance, in direct analogy to a conventional transistor.

Here we demonstrate the actuation of a unique, nano-scale radio frequency (rf) transistor which employs the Debye layer as its transduction element in a fundamentally novel way. The device comprises two nanofabricated electrodes embedded in a microfluidic channel, forming the transistor input and output, and a third gate electrode placed in the same fluid volume. The rf conductance between input and output is directly controlled by the gate voltage, which modulates the capacitance of the Debye layer formed on the input and output electrodes. The intrinsic large bandwidth of the Debye layer permits radio frequency gating of the transistor output, in our implementation to frequencies as high as 5 MHz, limited by the finite ionic conductance between the gate and the Debye layer. As a demonstration of the utility of this technique for studies in surface electrochemistry, as well as applications to impedance-based biosensing, we use it to quantitatively measure the Debye-layer capacitance, which allows us to measure the potential of zero charge (PZC) of the electrode surface.

The central element of the device consists of two nanofabricated gold interdigitated electrodes [IDEs, Fig. 1(a)], embedded in a poly-dimethylsiloxane-molded microfluidic channel containing an aqueous electrolyte [6]. The capacitance  $C_{DL}(V)$  of the electric double layer (EDL) that forms on these electrodes depends on the voltage difference  $V$  between the electrode and the solution. The rf conductance between the IDEs then depends on this voltage, which we control directly with a third gate electrode immersed in the

same electrolyte, as illustrated in Fig. 1(b). Unless otherwise noted, the electrolyte was 75 mM NaCl, and the gate electrode was a double-junction Ag/AgCl reference electrode (3M KCl) or, as we explicitly note for one experi-

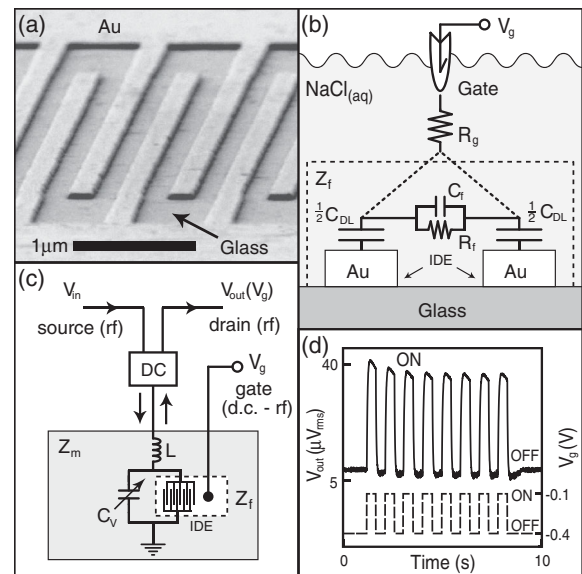


FIG. 1. (a) Scanning electron microscope image of portion of ten gold IDE fingers,  $200 \text{ nm} \times 40 \text{ nm}$ , separated by  $200 \text{ nm}$  and overlapping by  $20 \mu\text{m}$  in length, electron-beam lithographed on glass. (b) Gate voltage  $V_g$  is applied across the gate impedance  $Z_g$ : the electrolyte resistance  $R_g$  in series with the EDL capacitance  $C_{DL}$ . The rf impedance between IDEs is  $Z_f$ , boxed: the electrolyte response ( $R_f$  in parallel with  $C_f$ ), in series with the two  $V_g$ -dependent double-layer capacitances  $C_{DL}$ . (c) The rf source voltage of amplitude  $V_{in}$  is reflected from an rf impedance-matching circuit  $Z_m$ , which consists of an inductance  $L$ , a variable capacitor (varactor diode)  $C_v$ , and the IDE device. A directional coupler (DC) diverts the reflected rf signal, of amplitude  $V_{out}$ . (d) The rms voltage  $V_{out}$  (solid line) is plotted vs time as  $V_g$  (dashed line) is switched at 1 Hz between off ( $V_g = -400 \text{ mV}$ ) and on ( $V_g = -100 \text{ mV}$ ) values.

ment, a large-area ( $1600 \mu\text{m}^2$ ) gold electrode patterned next to the IDEs.

We connect the IDEs to a radio frequency impedance-matching circuit, which presents an impedance  $Z_m$  to an rf source, as shown in Fig. 1(c) [7]. The result is a transistor: The input (source) rf voltage  $V_{\text{in}}e^{i\omega t}$  incident on  $Z_m$  is reflected to the output (drain) as  $V_{\text{out}} = \Gamma V_{\text{in}}e^{i\omega t}$ , where  $\Gamma(Z_m)$  is the complex-valued reflectance [8], and  $\nu = \omega/2\pi = 50$  MHz unless otherwise noted. The gate voltage  $V_g$  controls  $V_{\text{out}}$  by changing the EDL capacitance  $C_{\text{DL}}$  and thus the rf conductance between the source and drain. In practice, we adjust the impedance-matching capacitance  $C_V$  [Fig. 1(c)] to minimize the reflectance for one value of the Debye capacitance  $C_{\text{DL}}$  (the off state), such that  $\Gamma = \Gamma_{\text{OFF}} \approx 0$ . A change in gate voltage changes  $C_{\text{DL}}$ , which increases the reflectance  $\Gamma$  and generates an increase in the output signal  $V_{\text{out}}$ , switching the transistor to the on state.

Transistor behavior is demonstrated in Figs. 1(d) and 2. In Fig. 1(d), we plot the output vs time as the gate voltage  $V_g \approx V$  is switched at 1 Hz between its off ( $V_g = -400$  mV) and on ( $V_g = -100$  mV) values. Figure 2 is the direct analog of the gate-dependent current-voltage characteristic of a conventional transistor [9], showing  $V_{\text{out}}$  vs  $V_{\text{in}}$  as a function of  $V_g$ . The inset in Fig. 2 shows the ratio  $|\Gamma(V_g)|/|\Gamma_{\text{OFF}}|$  vs  $V_g$ , the response due to the nonlinear dependence of  $C_{\text{DL}}$  on  $V$ , the voltage applied across the double layer [1]. We examine the broad dependence of  $C_{\text{DL}}$  on  $V_g$  in more detail below.

From two measurements we conclude that the Debye layer actuates this device: We show that the gate circuit impedance  $Z_g$  includes the EDL capacitance and that the voltage  $V$  across the EDL controls gating. The inset in Fig. 3 shows a typical direct measurement of  $|Z_g|$  as a function of frequency. The impedance is well approxi-

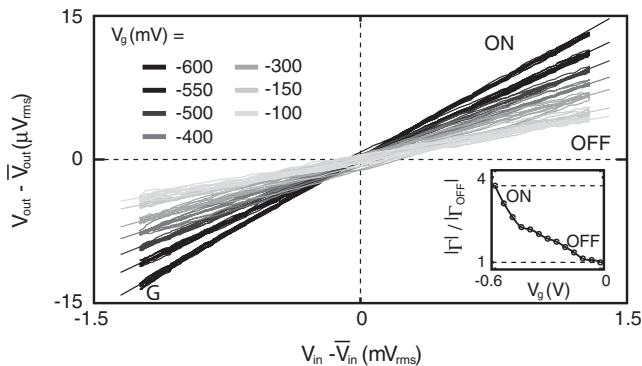


FIG. 2. Output voltage modulated by gate voltage. The rms amplitude  $V_{\text{out}} - \bar{V}_{\text{out}}$  vs  $V_{\text{in}} - \bar{V}_{\text{in}}$ , for several values of the gate voltage  $V_g$ . Each trace comprises five amplitude cycles of  $V_{\text{in}}$ , modulated at 1 kHz. We fit each trace to a straight line whose slope corresponds to the reflectance  $|\Gamma(V_g)|$ . The inset shows  $|\Gamma(V_g)|/|\Gamma_{\text{OFF}}|$  vs  $V_g$ . The shape of the curve is determined by the nonlinear voltage dependence of the EDL capacitance  $C_{\text{DL}}$  on  $V_g$ .

mated as the series combination of the electrolyte resistance  $R_g$  between the gate and the IDE, and the EDL capacitance  $C_{\text{DL}}$ . A least-square fit of  $|Z_g(f_g)|$  over frequencies  $f_g < 5$  Hz yields  $|Z_g| \propto 1/f_g^{0.87}$ , whereas an ideal RC circuit has a  $1/f$  dependence. This behavior is characteristic of the EDL capacitance [10], and the measured exponent is consistent with values reported elsewhere [11].

Using  $Z_g$ , we calculate a frequency-dependent EDL capacitance  $C_{\text{DL}}(f_g)$  which, together with the measurement of the electrode area  $A$ , yields the specific capacitance  $C_{\text{DL}}/A = 36 \mu\text{F}/\text{cm}^2$  at  $f = 5$  Hz. This value is within a factor of 2 of the Gouy-Chapman model for the EDL specific capacitance at this electrolyte concentration  $C/A \sim 60 \mu\text{F}/\text{cm}^2$  [1]. We conclude that the capacitance of the gate circuit is that of the EDL.

Second, we use a sinusoidal gate voltage and vary its frequency  $f_g$  to show that the voltage  $V$  developed across the double layer is what actually controls gating. The fraction of  $V_g$  that falls across the capacitor of a series RC circuit is frequency-dependent and is given by

$$\frac{V}{V_g} = \frac{1}{1 + i(f_g/f_{RC})}, \quad (1)$$

where  $f_{RC} = 1/(2\pi R_g C_{\text{DL}})$ . For  $f_g \ll f_{RC}$ ,  $V \approx V_g$  is maximal and in phase with  $V_g$ , while for  $f_g \gg f_{RC}$ ,  $V$  falls with frequency as  $V \propto V_g/f_g$  and lags  $V_g$  by a phase which approaches  $\pi/2$ . For gate actuation with the EDL, we expect corresponding changes in the modulation amplitude of  $V_{\text{out}}$  as  $V$  decreases in magnitude and changes its phase relative to  $V_g$ .

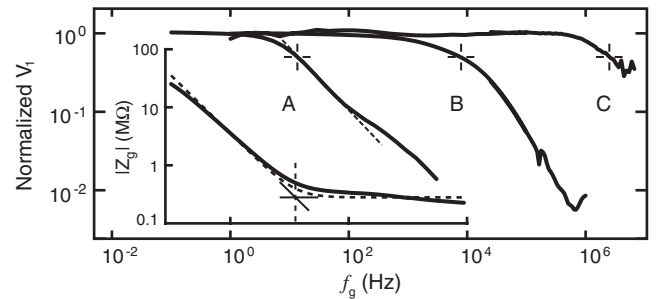


FIG. 3. Normalized amplitude of first harmonic in the output  $V_1(f)$  vs  $f_g$  for three different devices. Each exhibits a roll-off in amplitude at the corresponding  $f_{RC}$  of the gate impedance  $Z_g$ . A least squares fit to curve A between 15 and 80 Hz (dashed line) yields a dependence  $1/f_g^{0.8}$ . The inset shows  $|Z_g|$  vs  $f_g$  corresponding to curve A. For frequencies below  $f_{RC} = 1/(2\pi RC) \sim 10$  Hz (vertical dashed line), the EDL capacitance  $C_{\text{DL}}$  dominates  $Z_g$ , while above this frequency  $R_g$  dominates. The impedance of  $R = 300$  k $\Omega$  in series with an ideal capacitance of  $C = 45$  nF is shown by the curved dashed line. As  $R_g$  (curve B) or both  $R_g$  and  $C_{\text{DL}}$  (curve C) decrease, the roll-off frequency  $f_{RC}$  increases. Curve C shows gating of the device output ( $\nu = 100$  MHz) at  $f_g = 5$  MHz.

We measure the rms amplitude of the modulation of  $V_{\text{out}}$ ,  $V_1(f_g)$ , at the gate frequency  $f_g$  and plot the normalized  $V_1$  vs  $f_g$  in Fig. 3. Curve A is the output of the device whose gate impedance  $Z_g$  is shown in the inset and exhibits a pronounced roll-off at  $f_g \approx 10$  Hz, the same frequency as  $Z_g$ . The phase of the modulation of  $V_{\text{out}}$  relative to  $V_g$  also changes with  $f_{RC}$  in accordance with Eq. (1), shown in Fig. 4; for this device, operating in 1 mM NaCl,  $f_{RC} \approx 1$  Hz. The time dependence of  $V_{\text{out}}$  (solid lines) is shown together with  $V_g$  (dashed lines) for two different frequencies  $f_g$ . In (a),  $f_g = 0.2$  Hz  $< f_{RC}$ , and oscillations in  $V_{\text{out}}$  are in phase with  $V_g$ ; in (b),  $f_g = 5$  Hz  $> f_{RC}$ , and the phase is almost  $\pi/2$ . We conclude that the Debye layer actuates this device.

We measured two other device geometries and showed that  $f_{RC}$  changed as expected. We reduced the electrode area exposed to the fluid by a factor of  $\sim 10^3$  using a patterned dielectric layer, reducing  $C_{\text{DL}}$ , and increasing the roll-off frequency of  $V_1$  by the same factor of  $10^3$ , to  $\sim 8$  kHz (Fig. 3, curve B). Second, we moved the gate electrode to within  $\sim 5$   $\mu\text{m}$  of the IDEs by using an optically lithographed gold electrode as the gate. This decreased  $R_g$  and further increased the roll-off frequency to  $f_{RC} = 2.5$  MHz (Fig. 3, curve C). While the gold gate electrode introduces an additional EDL capacitance in series with the gate impedance,  $Z_g$ , its area was made large enough (1600  $\mu\text{m}^2$ ) that the effect of this capacitance was negligible. The data of Fig. 3 demonstrate gating of the device at 5 MHz, many orders of magnitude faster than nanofluidic transistors reported previously [5,12].

We can make quantitative measurements of  $C_{\text{DL}}$  using this device. We first use modeling to quantify the dependence of  $V_{\text{out}}$  on  $C_{\text{DL}}$ . We find that the response of the in-phase component  $I$  of  $V_{\text{out}}$  (referenced to  $V_{\text{in}}$ ) dominates in this operating regime, with responsivity

$$m \equiv \frac{\partial I}{\partial C_{\text{DL}}} \propto \frac{1}{2} \frac{1}{\omega^2 R_f C_f C_{\text{DL}}^2} \frac{1}{(1 + R_f/R_s)^2}, \quad (2)$$

where  $R_s$  is the equivalent parallel resistance due to loss in other circuit elements. Other measurements (not shown)

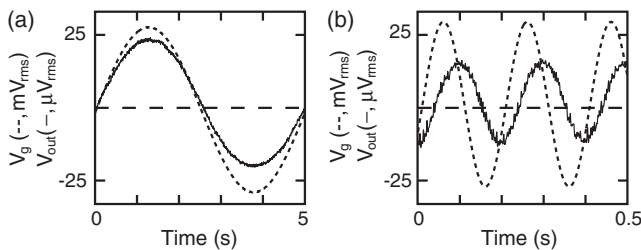


FIG. 4. Modulation of  $V_{\text{out}}$  (solid line) vs time with  $V_g$  (dashed line) for comparison. In (a),  $f_g = 0.2$  Hz  $< f_{RC}$ , and  $V_{\text{out}}$  oscillates in phase with  $V_g$ . In (b),  $f_g = 5$  Hz  $> f_{RC}$ , and  $V_{\text{out}}$  has phase  $-\pi/2$  with respect to  $V_g$ . Here the device was operating in 1 mM NaCl, with  $f_{RC} \approx 1$  Hz.

yield  $R_s \approx 8.9$  k $\Omega$ , and finite element modeling of the IDE geometry using the measured electrolyte conductance of 0.82 S/m yields  $R_f \sim 8$  k $\Omega$  and  $C_f \sim 0.8$   $\mu\text{F}/\text{cm}^2$ . With the measured specific capacitance of the double layer of 36  $\mu\text{F}/\text{cm}^2$  and the effective area of the overlapping IDE fingers, we obtain  $m \sim 160$   $\mu\text{V}/(\mu\text{F}/\text{cm}^2)$ , for  $V_{\text{in}} = 15.8$  mV<sub>rms</sub> at  $\omega/2\pi \approx 50$  MHz.

Because  $C_{\text{DL}}$  depends nonlinearly on the double-layer voltage  $V$  [1], a sinusoidal modulation of  $V_g$  at frequency  $f_g$  will generate modulation in  $V_{\text{out}}$  at the harmonics of  $f_g$ . When terms of higher order can be neglected, the first and second harmonic amplitudes of  $V_{\text{out}}$ ,  $V_1$  and  $V_2$ , respectively, can be used to calculate the first and second derivatives of  $C_{\text{DL}}$  with  $V$ ,  $C_1$  and  $C_2$ , respectively:

$$|C_1| \equiv \left| \frac{\partial C_{\text{DL}}}{\partial V} \right| = \frac{V_1}{|m|V_{\text{ac}}} \quad (3)$$

$$\text{and } |C_2| \equiv \left| \frac{\partial^2 C_{\text{DL}}}{\partial V^2} \right| = \frac{4V_2}{\sqrt{2}|m|V_{\text{ac}}^2},$$

where  $V_{\text{ac}}$  is the rms modulation amplitude of  $V_g$ . The overall signs of  $C_1$  and  $C_2$  are determined using  $\phi$ , the relative phase of the modulation in  $V_{\text{out}}$  with respect to  $V_g$ . For  $f_g < f_{RC}$ , we find that  $\phi \approx 0$  implies that  $\partial C_{\text{DL}}/\partial V < 0$ , whereas  $\phi \approx \pm\pi$  yields  $\partial C_{\text{DL}}/\partial V > 0$ .

We measure  $C_1$  and  $C_2$  as functions of  $\bar{V}_g$ , the mean value of  $V_g$ , and plot them in Fig. 5(a). The mean value of  $C_2$  about the maximum in  $C_1$ , 42.7  $\mu\text{F cm}^{-2} \text{V}^{-2}$ , has been subtracted to remove possible contributions from higher harmonics and noise. The phases  $\phi_1$  and  $\phi_2$  are plotted in Fig. 5(b); changes of  $\sim\pi$  indicate the zero crossings of  $C_1$  and  $C_2$ . To validate this method, we integrate  $C_2$  and set the

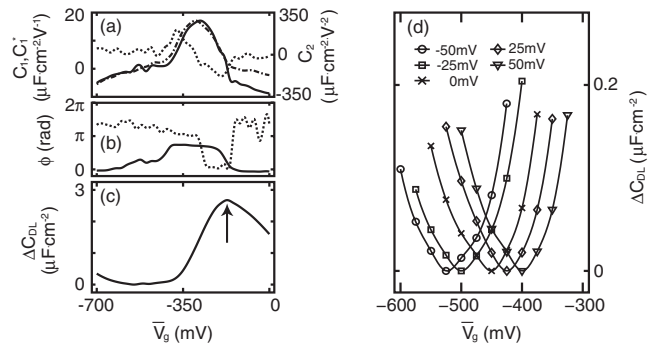


FIG. 5. (a)  $C_1$  (solid line),  $C_2$  (dashed line), and  $C_1^*$  (dotted-dashed line) are plotted vs  $\bar{V}_g$ . (b) The phases  $\phi_1$  of  $V_1$  (solid line) and  $\phi_2$  of  $V_2$  (dashed line) relative to  $V_g$  are plotted vs  $\bar{V}_g$ . Phase changes of  $\sim\pi$  are clear in both  $\phi_1$  and  $\phi_2$ , indicating the zero crossings of  $C_1$  and  $C_2$ , respectively. (c) Integrating  $C_1$  in (a) yields  $\Delta C_{\text{DL}}$ , which exhibits a peak at  $\bar{V}_g = -170$  mV (arrow). (d) Plot of  $\Delta C_{\text{DL}}$  vs  $\bar{V}_g$  as the IDEs are biased directly with voltage  $V_e$ . For each value of  $V_e$ ,  $C_1$  is approximately linear in  $\bar{V}_g$  and yields the quadratic  $C_{\text{DL}}$  minimum shown when integrated.  $C_{\text{DL}}$  depends only on the potential difference  $V_g - V_e$  across the EDL.

integration constant to match  $C_1$  at  $\bar{V}_g = -280$  mV. The result  $C_1^*$  is shown by the dotted-dashed curve in Fig. 5(a) and agrees well with  $C_1$ . We obtain  $C_{DL}$  by integrating  $C_1$  and plot the difference from its minimum value  $\Delta C_{DL}$  vs  $\bar{V}_g$  in Fig. 5(c). In Fig. 5(d), we plot  $\Delta C_{DL}$  vs  $\bar{V}_g$  as the IDE voltage  $V_e$  is varied directly, from  $-50$  to  $+50$  mV. Clearly,  $C_{DL}$  depends only on the potential difference  $V_g - V_e$  across the EDL.

The Debye layer forms in response to a net surface charge on the IDEs, which vanishes when the electrodes are biased at the PZC relative to the electrolyte. At the PZC, Gouy-Chapman theory [1] predicts a quadratic minimum in  $C_{DL}$ , as seen in Fig. 5(d) at  $+0.45$  V vs Ag/AgCl in aqueous NaCl.

The PZC of gold in nonadsorbing electrolytes is generally found in the range  $-0.15$  to  $0.35$  V vs Ag/AgCl [13]; the minimum we present here lies somewhat outside this range. However,  $Cl^-$  is well known to adsorb to gold [14] and shift the electrode potential presented to solution [1]. The  $C_{DL}$  minimum we observe is likely an indication of such a shifted PZC. We interpret the maximum at  $+0.17$  V vs Ag/AgCl as further evidence of  $Cl^-$  adsorption: Peaks in  $C_{DL}$  are expected at potentials of specific adsorption [15], and our data are consistent with the adsorption data of Ref. [16]. We observed no significant etching of the electrodes nor any steady-state faradaic currents over the course of measurements.

We have demonstrated the actuation of a novel radio frequency transistor with the electrolytic Debye layer at frequencies up to 5 MHz. The sensitivity of this device to gate-voltage induced changes in the EDL capacitance, with a time resolution of order 100 ns, means it could be used to study fast-rate processes affecting the Debye layer in real time, such as molecular binding to the electrode surface. On bare gold electrodes we have measured the voltage dependence of the EDL capacitance, finding a peak in  $C_{DL}$  at  $+0.17$  V vs Ag/AgCl, which we suggest is caused by  $Cl^-$  adsorption, and a quadratic minimum indicating the PZC at  $+0.45$  V vs Ag/AgCl. The same technique could be used to study the ionic behavior at the surface of a dielectric coating of metal electrodes. Some molecules exhibit enhanced binding to electrodes biased at the PZC [17], and binding, in general, of charged molecules is affected by residual surface charge. The ability of this device to determine the PZC of a wide variety of materials *in situ* is therefore highly relevant to impedance-based molecular biosensing applications.

This research was supported by an NIH PEN grant “Nanotherapies for Vulnerable Plaque” and the Center

for Nanoscience Innovation for Defense. The authors thank Chris McKenney for valuable discussion and his tireless maintenance of the SEM and Bob Hill for technical support. We acknowledge use of the UC Santa Barbara Nanofabrication Facility, supported in part by the NSF and the National Nanofabrication Infrastructure Network.

- 
- [1] A. J. Bard, *Electrochemical Methods Fundamentals and Applications* (Wiley, New York, 1980), 2nd ed.
  - [2] R. Riehn, R. Austin, and J. Sturm, *Nano Lett.* **6**, 1973 (2006); A. Ajdari, *Phys. Rev. Lett.* **75**, 755 (1995); I. M. Lazar and B. L. Karger, *Anal. Chem.* **74**, 6259 (2002); S. Pennathur and J. Santiago, *Anal. Chem.* **77**, 6782 (2005); J. Yang *et al.*, *J. Micromech. Microeng.* **13**, 963 (2003); F. H. J. van der Heyden, D. Stein, and C. Dekker, *Phys. Rev. Lett.* **95**, 116104 (2005).
  - [3] E. Kalman, I. Vlasiouk, and Z. Siwy, *Adv. Mater.* **20**, 293 (2008).
  - [4] Z. Siwy *et al.*, *J. Am. Chem. Soc.* **126**, 10 850 (2004).
  - [5] R. Fan *et al.*, *Phys. Rev. Lett.* **95**, 086607 (2005).
  - [6] D. Duffy *et al.*, *Anal. Chem.* **70**, 4974 (1998).
  - [7] D. K. Wood, M. V. Requa, and A. N. Cleland, *Rev. Sci. Instrum.* **78**, 104301 (2007); D. K. Wood *et al.*, *Lab Chip* **7**, 469 (2007); D. K. Wood *et al.*, *Appl. Phys. Lett.* **87**, 184106 (2005); G. R. Facer, D. A. Notterman, and L. L. Sohn, *Appl. Phys. Lett.* **78**, 996 (2001).
  - [8] D. M. Pozar, *Microwave Engineering* (Wiley, New York, 1998), 2nd ed.
  - [9] P. Horowitz, *The Art of Electronics* (Cambridge University Press, Cambridge, England, 1989), 2nd ed.
  - [10] T. Pajkossy, *Solid State Ionics* **176**, 1997 (2005); L. Nyikos and T. Pajkossy, *Electrochim. Acta* **30**, 1533 (1985); T. Pajkossy, T. Wandlowski, and D. M. Kolb, *J. Electroanal. Chem.* **414**, 209 (1996).
  - [11] A. Sadkowsky, A. J. Motheo, and R. S. Neves, *J. Electroanal. Chem.* **455**, 107 (1998).
  - [12] I. Vlasiouk and Z. Siwy, *Nano Lett.* **7**, 552 (2007); S. Umehara *et al.*, *Nano Lett.* **6**, 2486 (2006); R. Karnik, K. Castelino, and A. Majumdar, *Appl. Phys. Lett.* **88**, 123114 (2006).
  - [13] A. Hamelin *et al.*, *J. Electroanal. Chem.* **145**, 225 (1983).
  - [14] S. Biggs *et al.*, *J. Am. Chem. Soc.* **116**, 9150 (1994).
  - [15] B. E. Conway, *Prog. Surf. Sci.* **16**, 1 (1984); S. B. Emery, J. L. Hubble, and D. Roy, *Electrochim. Acta* **50**, 5659 (2005).
  - [16] W. K. Paik, M. A. Genshaw, and J. O. Bockris, *J. Phys. Chem.* **74**, 4266 (1970).
  - [17] M. Rohwerder, K. de Weldige, and M. Stratmann, *J. Solid State Electrochem.* **2**, 88 (1998); D. Bizzotto and J. Lipkowsky, *J. Electroanal. Chem.* **409**, 33 (1996).